The dynamics of exciton tunneling and trapping in condensed xenon on ultrafast time scales

Eric S. Peterson,[a] Benjamin J. Schwartz,[b] and Charles B. Harris
Department of Chemistry, University of California, Berkeley, California 94720 and Chemical Sciences Division, Lawrence Berkeley Laboratory, Berkeley, California 94720

(Received 23 December 1992; accepted 14 April 1993)

We report the use of picosecond transient absorption spectroscopy to directly observe the dynamics of formation, tunneling, and subsequent cooling of the $n=1$, $\Gamma(3/2)$ exciton in condensed xenon over a density range of 0.10 to 1.8 g/ml. At lower densities, only Xe_2^* excimers are formed, which undergo vibrational cooling on a tens of picoseconds time scale. At densities high enough to support exciton formation, tunneling from the free to the trapped exciton state takes place in $\leqslant 3$ ps, and cooling of the localized exciton takes place in 5–10 ps; neither rate is strongly dependent on Xe density over the range investigated. The results are compared to theories that describe the formation and cooling rates of the trapped exciton state, and are consistent with a resonant energy transfer mechanism in which the excitation hops between neighboring Xe atoms during the trapping process.

I. INTRODUCTION

Since the pioneering work of Frenkel[1] and Wannier[2] in the 1930s, the concept of an exciton[3] has become central to theories of the electronic structure of rare gas solids.[4,5] Subsequent efforts by Jortner and Rice[6,7] established the importance of excitonic states in rare gas liquids as well as in crystals. Excitons in the condensed rare gases exist in either a free state, delocalized over an entire crystal, or in a trapped state, delocalized over just a few atomic sites. Excitons have been successfully used to explain the absorption,[8] reflection,[9–11] luminescence,[12–14] and transient absorption[15] spectra of condensed rare gases. More recently, the evolution of excitonic states from the corresponding gas phase excitations has been studied as a function of density and temperature[16] as well as impurity and defect concentration,[17] leading to a better understanding of the energetics and dynamics involved in exciton formation and trapping.

As delocalized entities, excitons encompass multiple atomic sites and hence, are sensitive to the presence of defects in the crystal or the local structure of a liquid.[16,18] As the density of a rare gas is increased, there is a threshold at which the average size of the rare gas atom clusters in the fluctuating fluid becomes equal to the radius of the delocalized exciton. Only above this critical density can these fluids support the formation of excitons.[10,11,19] This idea of an exciton critical density is born out by the order of appearance of the $\Gamma(3/2)$ $n=1$ and $n=2$ excitons in liquid xenon: The $n=1$ exciton, which has a radius of 2.7 Å, appears at densities above 100 amagats (density units in this paper convert as follows: 1.0 amagat $=2.7\times10^{19}$ atoms/cm^3 $=5.9\times10^{-3}$ g/ml for Xe) while the $n=2$ exciton, which has a radius of 11 Å, does not appear until the density is greater than 400 amagats.[11]

For condensed xenon, the lowest energy exciton, the $n=1$ exciton of the $\Gamma(3/2)$ series at 8.36 eV, arises from delocalization of the $5p^6\rightarrow 6s(3/2)_1^0$ atomic transition.[5,8] Excitation of this exciton at 8.36 eV results in emission at 8.36, 7.6, and 7.2 eV, indicative of a trapping mechanism which can strongly stabilize the exciton. The emission at 8.36 eV arises from the free exciton state. Early work attributed the 7.2 and 7.6 eV emission to the $n=1$ and $n=2$ excitons of the $\Gamma(3/2)$ series, respectively.[12] Subsequent temperature dependent studies, however, have assigned the 7.2 eV emission to excitons trapped at a lattice vacancy defect and the 7.6 eV emission to excitons trapped in the bulk fcc lattice.[13,16] Lattice deformation calculations indicate the presence of a $\sim$0.035 eV barrier separating the free exciton state from the trapped exciton state.[20] Once over the barrier, the trapped excitons are localized to a few atomic sites, and behave essentially as gas phase xenon excimers (Xe_2^*) solvated in the bulk xenon.[7] Martin has proposed a trapping mechanism whereby the exciton loses energy to the lattice via a resonantly enhanced energy transfer process consisting of consecutive hops of the atomic excitation from one site to another during a collision with the lattice.[14] With each collision, the excitation loses more energy to the lattice. Martin's calculations indicate that only a few collisions are necessary for the exciton to lose $\geqslant$0.5 eV of energy, implying that the exciton trapping rate is on the order of 10^{12} s^{-1}. Because of this extremely high rate, there have been no direct room temperature measurements of either the exciton trapping rate or the tunneling rate of the free excitons through the barrier to the trapped exciton well.

In this paper, we report the use of picosecond transient absorption spectroscopy to directly observe the dynamics of formation, tunneling and subsequent cooling of the $\Gamma(3/2)$ $n=1$ exciton in supercritical and liquid xenon near room temperature. We examine these processes as a function of density and follow the evolution of excitation relax-

[a]Present address: Albert Einstein College of Medicine, Department of Physiology and Biophysics, 1300 Morris Park Avenue, Bronx, NY 10461.
[b]Present address: Department of Chemistry and Biochemistry, University of Texas, Austin, TX 78712.

 0021-9606/93/99(3)/1693/10/$6.00

ation from the simple cooling of gas phase xenon excimers at low densities to the formation and trapping of the $\Gamma(3/2)$ exciton as the density is increased. We then discuss the implications of these results in a general picture of the behavior of electronic excitations in condensed rare gases.[21]

II. EXPERIMENT

A. Picosecond laser system

The laser system used for the picosecond transient absorption experiments has been described previously.[22] Briefly, a mode-locked argon ion laser synchronously pumps a dye laser to produce 1–2 ps pulses at 590 nm. These pulses are then amplified in a three stage dye cell amplifier pumped longitudinally by a 10 Hz, Q-switched Nd:YAG laser. The final output consists of pulses ~ 1 ps in duration with ~ 1 mJ/pulse at 10 Hz. This light is doubled in a 1 mm thick KDP crystal to produce 0.1 mJ excite pulses at 295 nm. The residual fundamental light is focused into a 5 cm cell containing water or acetone to generate a white-light picosecond continuum. Bandpass filters are used to select a 10 nm FWHM portion of the continuum for use as the probe light.

The 295 nm pump pulses were sent through a variable double-pass optical delay line with 10 μm (67 fs) resolution before arriving at the sample. The probe light was split into signal and reference beams, collected on large area photodiodes (EG&G DT-110) and processed by a 386 computer controlled gated integrator. Probe light levels outside the linear response regime of the detection system were rejected from data collection. Data were normalized on every laser shot with a typical spread in the normalized ratios for 100 shots of 0.2% (± 1 standard deviation).

Transient absorption data was collected in the following manner: For each delay, 20 normalized laser shots were averaged for a single data point, the delay between the pump and probe pulses changed, and then another 20 laser shots were averaged at the new stage position and so on until an entire scan was complete. In the results presented below, 10–50 of these scans were averaged together (200–1000 total averaged laser shots) with the stage moving in opposite directions on alternating scans to remove long-term drift artifacts.

The pump and probe beams passed through the sample collinearly. Since large pump intensities lead to multiphoton excitation of the sapphire cell windows resulting in large interfering transient absorption signals, the pump intensity was attenuated with neutral density filters until no signal was seen from the empty cell. The typical pump energies used in the experiments were 3–10 μJ. Average signal sizes obtained in this manner were absorbance changes on the order of 1%. The time resolution of the system was determined by cross correlation of the visible and UV pulses as the transient absorption rise of diphenylbutadiene in hexane and was fit to a 1.2 ps Gaussian.

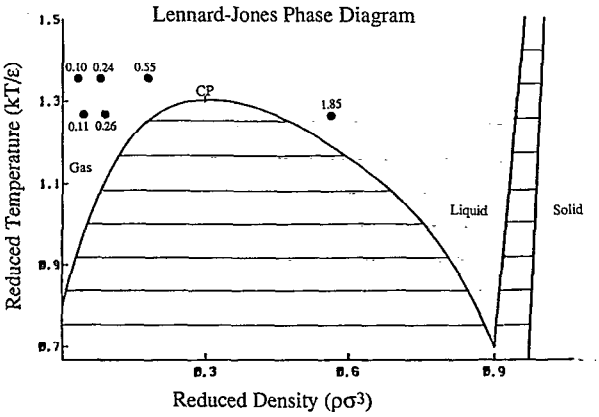

FIG. 1. Lennard-Jones phase diagram. The solid circles indicate the densities and temperatures used in the experiments for Lennard-Jones xenon (σ=4.1 Å, ϵ=154 cm^{-1}), the numbers indicate the density in g/ml. The highest density point (1.85 g/ml at 810 psi and 280 K) falls clearly into the liquid region. Two of the remaining five points (0.11 and 0.26 g/ml at 280 K and 250 or 500 psi, respectively) fall distinctly into the gaseous region. The remaining three points (0.10, 0.24, and 0.55 g/ml at 295 K and 250, 500, or 810 psi, respectively) are above the xenon critical point (CP), falling in the supercritical fluid region of the phase diagram.

B. Sample preparation

For all the experiments, the sample was neat xenon (Airco, 99.995%), used without further purification, confined at the desired temperature and pressure in a homemade optical cell.[21] The cell consists of a machined 316 stainless steel body, with optical access provided by two 2 mm thick sapphire windows (Janos or Melles Griot) sealed with Al and Cu gaskets and a teflon O-ring. The optical path length is 1 cm, providing a sample volume of a few ml of condensed xenon. Pressure in the cell was regulated from 0 to 1200 psi by leaking xenon from a high pressure reservoir (in which the xenon had been cryogenically condensed and allowed to reequilibrate at room temperature) into the cell in a controlled fashion. Sample temperature was maintained by a circulating chilled water/ethylene glycol bath (Neslab) in thermal contact with the cell body. Liquid xenon was confirmed present in the cell at high pressures and low temperatures by the visual observation of a meniscus during filling. The phase diagram of xenon is well known and has been fit to several equations of state; the density of xenon confined at a given temperature and pressure was computed from either the Strobridge or the Beattie–Bridgeman equations of state.[23] Figure 1 shows the reduced phase diagram for Lennard-Jones xenon (σ=4.1 Å, ϵ=154 cm^{-1}); the solid circles in the figure mark the six conditions at which the experiments were performed.

The presence of parts per million impurities in liquid xenon can affect electronic excitation lifetimes and mobilities. Thus, all parts of the cell and gas handling system exposed to the xenon were either electropolished or ultrasonically cleaned in hexane to remove oils and ensure the purity of the sample. The presence of very low levels of impurities in the sample was observed in the variation of the long ($\sim$20 ns) decay time of the transient absorption

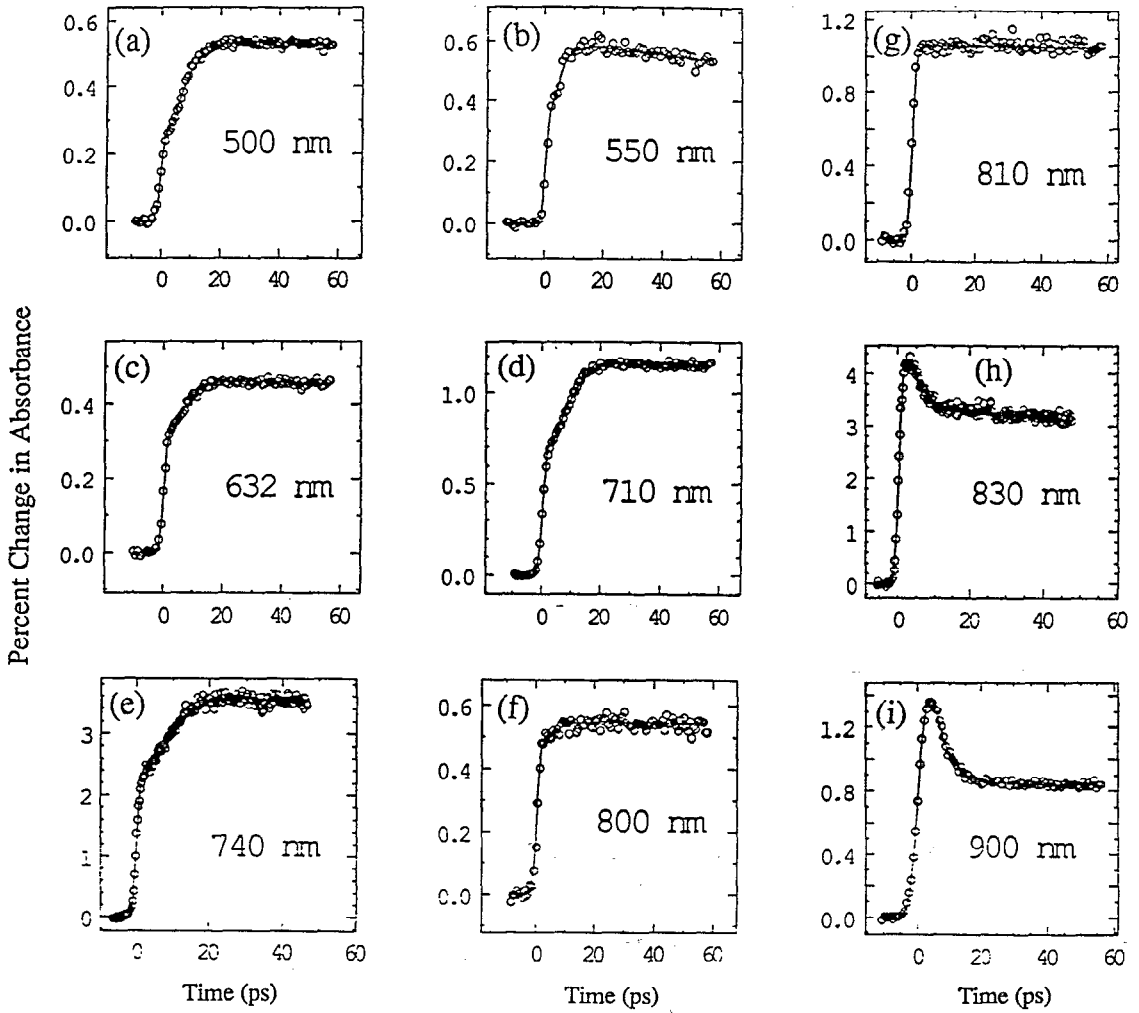

FIG. 2. Transient absorption dynamics for xenon at 810 psi and 280 K (1.85 g/ml) on the 1 to 60 ps time scale at various probe wavelengths. Circles are data points, solid lines are fits to Eq. (1) with parameters summarized in Table I. The ordinate shows percent change in absorbance.

signal from run to run, indicating diffusion of the electronic excitation to impurity sites and subsequent quenching. All the short time ($\leqslant$100 ps) scans discussed below were completely reproducible, even when known oil impurities were introduced into the sample, confirming that diffusion and trapping at impurity sites is not important on the picosecond time scale.

III. RESULTS

In order to probe the dynamics of exciton formation, tunneling and trapping, we have used picosecond transient absorption spectroscopy to observe the decay of the free exciton and the subsequent growth and cooling of the trapped exciton in condensed xenon. The $n=1$ exciton of the $\Gamma(3/2)$ series (8.36 eV) was two-photon excited by the 295 nm (4.2 eV) picosecond pump pulse, and the resulting dynamics were probed at wavelengths spanning the visible and near IR spectral regions. Typical picosecond transient scans at different wavelengths are shown in Fig. 2. The data are plotted as the percent change in sample absorbance as a function of delay time between the pump and probe pulses in ps ($\Delta A=-\log[I/I_0]$, where I_0 is the intensity of the probe pulse before the sample, and I is the intensity of the probe pulse after the sample). The solid lines through the data are fits to a simple first-order kinetic model in which one absorbing population is decaying while a second absorbing species is growing in intensity:

$$\Delta A=C_1\exp[-t/\tau_1]+C_2(1-\exp[-t/\tau_2]). \qquad (1)$$

The function in Eq. (1) is convoluted with an $\sim$1.2 ps Gaussian representing the instrument function. The fitting parameters τ_1, τ_2 and the ratio C_1/C_2 for all the scans of Fig. 2 are summarized in Table I. The transient absorptions for all the scans decay to zero after $\sim$20 ns, indicating the disappearance of the second absorbing species on this long time scale. This process does not affect the dynamics observed over the 100 ps duration of the short scans of Fig. 2 and, hence, is not represented in Eq. (1). As mentioned above, the lifetime of this species is sensitive to the presence of impurities in the sample, and varied from run to run.

At a constant density of 1.85 g/ml$=8.46\times10^{21}$ atoms/cm$^3=313$ amagats (xenon at 810 psi and 280 K), transient absorption dynamics were measured at 500, 550,

TABLE I. Fit parameters[a] for Xe transient absorption at 1.85 g/ml[b] (Fig. 2).

Probe wavelength (nm)	C_1/C_2	τ_1 (ps)	τ_2 (ps)
500	0.62	0.9	6.5
550	0.48	2.0	5.2
632	0.66	2.0	4.4
710	0.59	2.1	6.1
740	0.76	2.4	5.7
800	0.77	2.1	2.9
810	1.0	c	c
830	0.93	3.3	2.0
900	2.2	4.2	3.2

[a]Fit to $\Delta A = C_1 \exp[-t/\tau_1] + C_2\,(1-\exp[-t/\tau_2])$ convoluted with a 1.2 ps Gaussian representing the instrument function. Estimated uncertainties in parameters C_1/C_2: ± 0.15, τ_1 and τ_2: ± 1 ps.
[b]Liquid Xe confined at 810 psi and 280 K; $\rho = 1.85$ g/ml $= 8.46 \times 10^{21}$ atoms/cm^3.
[c]Data for 810 nm was flat on the 100 ps time scale, indicating that $\tau_1 = \tau_2$. Determination of a unique value is not possible.

632, 710, 740, 800, 810, 830, and 900 nm [Figs. 2(a)–2(i)]. The scans of Figs. 2(a)–2(f) all show an instrument limited ($\leqslant$1.2 ps) initial rise, followed by a slower rise on 3–7 ps time scale, indicating that the ratio C_1/C_2 is <1 for these wavelengths. The sharp breaks or wiggles in the transient absorption after the initial rise, most visible in the 500, 632, 710, and 740 nm scans [Figs. 2(a), 2(c)–2(e)] are due to a fast, $\leqslant$3 ps decay component which has been convoluted with the rise by the instrument function. At the reddest probe wavelengths, Figs. 2(h) and 2(i), the scans show an instrument limited rise followed by the fast decay, indicating that the ratio C_1/C_2 is >1. The most unique trace occurs at 810 nm, shown in Fig. 2(g). This scan has an instrument limited initial absorbance rise, and then the absorbance does not change for many nanoseconds. In terms of the parameters of Eq. (1), this means that $C_1/C_2 = 1$ and $\tau_1 = \tau_2$ for this wavelength. The absolute cross section of the transient absorption appears to continuously increase to redder wavelengths; a more quantitative statement is not possible, however, as the spatial overlap between the pump and probe pulses varies with wavelength, making absolute absorbance comparisons between different wavelengths difficult.

To examine the density dependence of the excitonic behavior, transient absorption scans at the bluest and reddest wavelengths, 500 and 900 nm, were taken at a variety of xenon densities by varying the pressure, and to a lesser extent, the temperature of the sample. Figure 3 shows 900 nm transient absorption dynamics for xenon at densities of 0.10, 0.11 g/ml (250 psi and 294 or 280 K, respectively), 0.24, 0.26 g/ml (500 psi and 294 or 280 K, respectively) and liquid xenon at 1.8 g/ml. For the four lower density scans, the absorptions are fit to a simple kinetic model indicating the appearance and disappearance of a single absorbing species:

$$\Delta A = C_3(1-\exp[-t/\tau_3])\exp[-t/\tau_4]. \qquad (2)$$

The fit parameters for these four scans are summarized in Table II. As the density is increased, the absorbing species

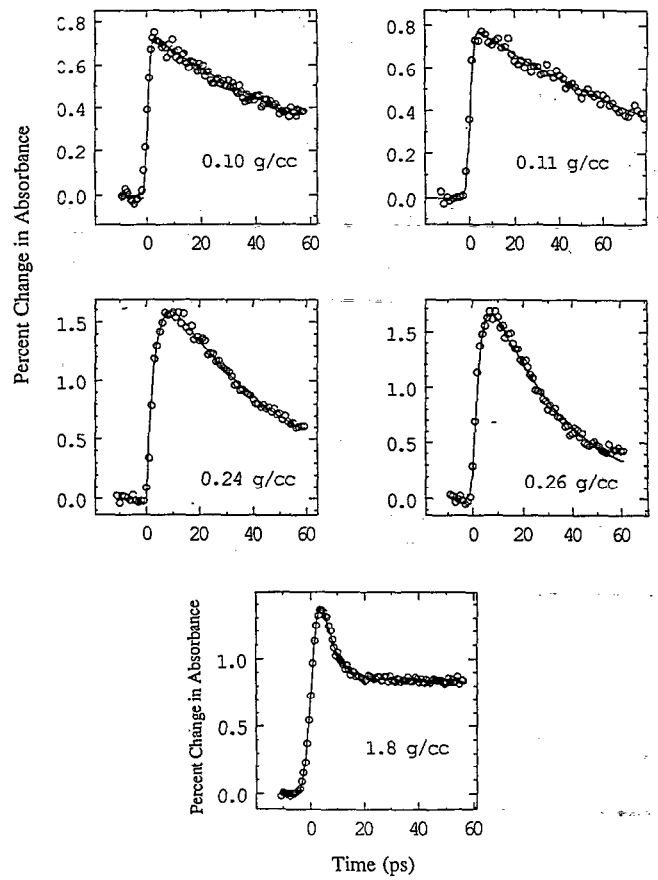

FIG. 3. Transient absorption dynamics at 900 nm for xenon at various densities. The solid lines in the four low density scans are fits to Eq. (2) with parameters summarized in Table II; the 1.8 g/ml scan, the same as in Fig. 2(i), is shown for comparison.

takes more time to appear and decays away more quickly. At the liquid density of 1.8 g/ml, as discussed above, two absorbing species are needed to successfully model the absorption dynamics. Figure 4 shows 500 nm transient absorption data taken for xenon densities of 0.55 and 1.8 g/ml (810 psi and 294 or 280 K, respectively). The fits to Eq. (1) for these scans are virtually identical within the noise, as summarized in Table III.

To learn more about the nature of the initial excitation, experiments were done that varied the wavelength and in-

TABLE II. Fit parameters[a] for 900 nm transient absorption of Xe at different densities (Fig. 3).

Density (g/ml)	Density (atoms/cm^3)	Temperature (K)	Pressure (psi)	τ_3 (ps)	τ_4 (ps)
0.10	4.7×10^{20}	295	250	b	75
0.11	5.0×10^{20}	280	250	b	72
0.24	1.1×10^{21}	295	500	3.4	46
0.26	1.2×10^{21}	280	500	2.9	31

[a]Fit to $\Delta A = C_3(1-\exp[-t/\tau_3])\exp[-t/\tau_4]$ convoluted with a 1.2 ps Gaussian representing the instrument function. Estimated uncertainties in parameters τ_3: ± 1 ps, τ_4: ± 5 ps.
[b]Rise time less than the 1.2 ps instrument function.

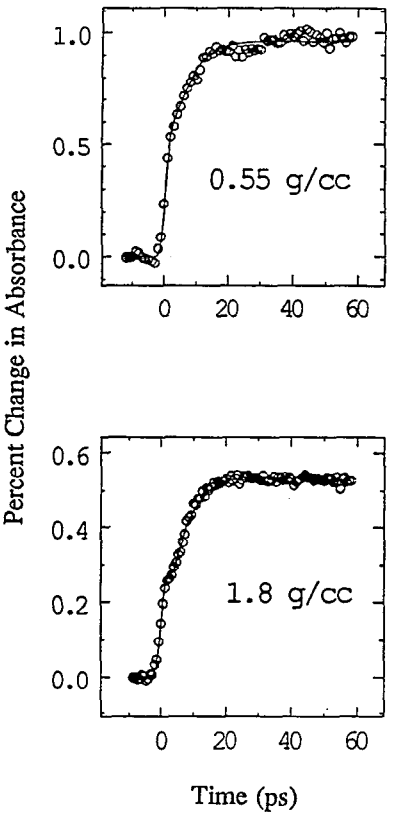

FIG. 4. Transient absorption dynamics at 500 nm for xenon at two different densities. The solid lines are fits to Eq. (1) with identical parameters, as summarized in Table III. The 1.8 g/ml scan is that same as that shown in Fig. 2(a).

tensity of the excite pulses. No change in transient absorption dynamics was observed when the excite wavelength was changed from 295 to 292 nm. Power dependence experiments indicated that the amplitude of the transient signal was proportional to $I^{\sim 1.5}$, where I is the intensity of the 295 nm excite pulses. Only the magnitude of the transients, not their shapes or decay times, changed with changing pump intensity. In an effort to ascertain whether or not three-photon excitation of the Xe occurred, an additional experiment with an intensified reticon array searched for fluorescence from the sample in the 800–900 nm region, indicative of processes in the $6p$ electronic manifold of atomic Xe.[24,25] Fluorescence from the sapphire windows could be seen with maximum UV pump intensity, but no emission was observed from the xenon sample.

TABLE III. Fit parameters[a] for 500 nm transient absorption of Xe at different densities (Fig. 4).

Density (g/ml)	Density (atoms/cm^3)	Temperature (K)	Pressure (psi)	C_1/C_2	τ_1 (ps)	τ_2 (ps)
0.55	2.5×10^{21}	295	810	0.45	2.0	5.2
1.85	8.5×10^{21}	280	810	0.62	1.0	6.5

[a]Fit to $\Delta A = C_1 \exp[-t/\tau_1] + C_2(1-\exp[-t/\tau_2])$ convoluted with a 1.2 ps Gaussian representing the instrument function. Estimated uncertainties in parameters C_1/C_2: ± 0.15, τ_1 and τ_2: ± 1 ps.

IV. DISCUSSION

A. Picosecond creation of excitons in condensed xenon

In most of the previous work on rare gas excitons, excitation was accomplished with either high energy particles or synchrotron radiation. Neither of these methods, however, provides time resolution sufficient to directly examine exciton formation and trapping dynamics. By taking advantage of the high peak powers and time resolution offered by ultrashort laser pulses, excitons in liquid xenon can be created coherently by multiphoton excitation on a picosecond time scale, providing the opportunity to study the resulting tunneling and trapping dynamics directly. Multiphoton excitation also allows the use of sapphire windows in the sample cell which are opaque to the vacuum ultraviolet radiation from synchrotrons. The high tensile strength of sapphire windows allows access to the room temperature regime where high pressures are necessary to compress xenon to densities sufficient for the study of excitonic behavior. Previous studies have been constrained to cryogenic temperatures associated with lower pressures. Thus, the high peak intensities associated with picosecond laser pulses allow the study of rapid relaxation processes which occur near room temperature.

This high peak intensity, in addition to creating excitons, could also cause multiphoton ionization or dielectric breakdown in the sample. The power dependence experiments show that the transient absorption amplitude scales with the excite laser intensity to the ~ 1.5 power. This merely reveals that the excitation was well into the saturation regime, a behavior which has been previously observed in multiphoton excited processes in the rare gases.[26] The only conclusion that can be drawn is that the observed signals are the result of a more than one photon process; whether the excitation involves two and/or three photons cannot be determined from the power dependence.

Two photons at 295 nm (4.2 eV) are energetically resonant with the $5p^6 \rightarrow 6s(3/2)_1^0$ atomic xenon transition from which the $\Gamma(3/2)$ $n=1$ exciton evolves in the condensed phase. In the gas phase, this $\Delta l=1$ transition is forbidden in the dipole approximation ($\Delta l=0$ or 2 is allowed). In a condensed environment, however, perturbations from neighboring xenon atoms can break this two-photon selection rule; even in a low density gas, ground state xenon atoms which are close enough together can be directly two-photon excited to form a Xe_2^* excimer.[27]

Three-photon excitation of xenon at 295 nm (12.6 eV) is also possible and would exceed the ionization limit of the atom in the gas phase (12.13 eV).[28] In the condensed phase, the ionization threshold of Xe is lowered due to stabilization of the ion and electron by the surrounding media; therefore, the photoelectron produced after 12.6 eV excitation should have $\geqslant 0.5$ eV excess energy. Since photoionization cross sections generally decrease with increasing photon energy above threshold, three-photon excitation of xenon at 295 nm should have a small absolute cross section. (The photoejected electron's wave function becomes increasingly oscillatory with increasing energy above

threshold, leading to poorer overlap with the initial bound state and thus to a decreasing photoionization cross section with increasing excess energy. This effect becomes important when the wavelength of the ejected electron becomes smaller than the size of the atom. For 0.5 eV electrons, the deBroglie wavelength is ~1 Å.) Thus, the probability of absorbing a third 295 nm photon to ionize the xenon after the absorption of the first two photons to create the exciton should be much lower than the probability of making the direct two-photon absorption. This suggests that the signals observed in our experiments are dominated by excitons created via two-photon (8.4 eV) absorption rather than ions and electrons produced from three-photon (12.6 eV) excitation.

Further evidence that the observed transient absorption signals are not the result of three-photon absorption is provided by the lack of emission between 800 and 900 nm. Ionization of xenon in the condensed phase is rapidly followed by recombination of the electrons with Xe^+ or Xe_2^+ ions which eventually produces highly excited Xe atoms.[25] One of the dominant relaxation mechanisms of highly excited atomic xenon in the gas phase is strong emission near 830 nm from the $6p \rightarrow 6s$ manifolds.[24,25] In the experiment described above, no fluorescence was observed in this region. This result is consistent with the fact that xenon atoms are not being excited above the $6p$ manifold by the 295 nm picosecond laser pulses. (There are several possible alternative explanations for this negative result. First, 830 nm fluorescence could be present but with a yield below our detection sensitivity. Second, a quenching mechanism could be present in the condensed phase preventing this signature of higher excitation. Similar quenching has been observed in previous studies, such as those in Ref. 24.) All of the results are consistent with the conclusion that the excitation mechanism is the direct two-photon resonant creation of either the $\Gamma(3/2)$ $n=1$ exciton at the higher densities or the diatomic xenon excimer at the lower densities.

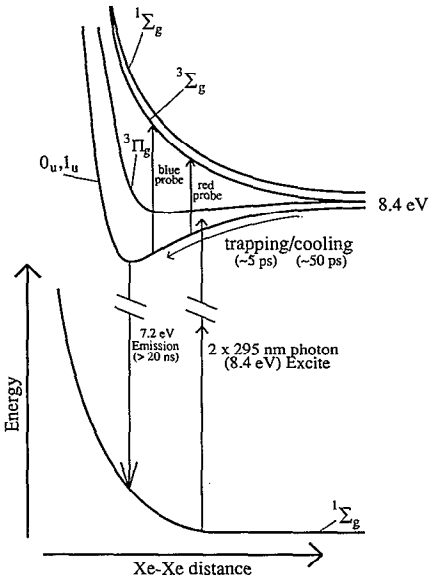

FIG. 5. Energy level schematic showing Xe–Xe pair interactions. Two 295 nm photons excite a pair of Xe atoms which are at their van der Waals' separation to an excited bound state near 8.4 eV. Vibrationally hot excimers/trapped excitons absorb to the red of vibrationally cool excimers, leading to a blue shift of the transient absorption spectrum with time. After complete (~0.65 eV) cooling, trapped excitons/cool excimers can emit 7.2 eV photons, returning to a repulsive region (~0.5 eV above the energy at infinite separation) on the ground state potential energy surface.

B. Exciton tunneling and trapping dynamics

The $\Gamma(3/2)$ $n=1$ exciton has been characterized by luminescence which occurs at 8.36, 7.6, or 7.2 eV, depending on the temperature and crystallinity of the sample. The 8.36 eV emission line is from the free exciton, the two Stokes shifted lines are emission from excitons trapped at either bulk lattice sites or lattice defects.[13,16] Since the trapped exciton is similar in structure to the gas phase excimer, part (~0.5 eV) of the observed Stokes shift is attributed to the repulsive energy of the two xenon atoms on the ground state at the excited state interatomic separation (Fig. 5). The remaining portion of the Stokes shift (~0.25 or ~0.65 eV) is due to stabilization by excited state trapping. To provide this stabilization, the surrounding lattice must undergo significant deformation, leading to a barrier for formation of the trapped exciton from the free exciton.[16,20] This concept is illustrated schematically in Fig. 6; calculations estimate the height of this barrier to be ~35 meV.[20] The initially excited free exciton state is a shallow well which is not strongly coupled to lattice deformations. Upon crossing the barrier, however, the lattice can deform to stabilize the free exciton by an additional ~0.5 eV. The tunneling times through this barrier can vary from a few nanoseconds in near perfect xenon crystals at low temperatures to an estimated few picoseconds for disordered solid or liquid xenon. (In the literature, the term "trapping rate" is often used to describe the time for the tunneling decay of the free exciton since the trapping occurs essentially instantaneously after tunneling, which can occur on the ns time scale at low temperatures. For example, the "trapping rates" quoted in Ref. 18 refer to decay from the free exciton well. In this paper, we confine the use of the term "trapping" to cooling of the exciton in the trapped state well and refer to motion of the exciton from the free state to the trapped state as tunneling.) Once across the barrier, the time for cooling in the trapped state well should be on the order of a few ps, as estimated by Martin with a resonantly enhanced hopping mechanism for xenon between 50 and 150 K.[14] The results discussed herein represent the first direct observation of exciton tunneling and trapping in room temperature liquid xenon.[21]

The transient absorption data for liquid xenon shown in Fig. 2 fit well to Eq. (1), a simple model in which one absorbing species decays while a new absorbing species grows in on a similar time scale. Based on the time scales observed in the experiment, the logical assignment is that the two species are the free and trapped $n=1$, $\Gamma(3/2)$ exciton. The fit parameters of Table I can then be simply interpreted: τ_1 is the lifetime of the free exciton, essentially the tunneling time through the barrier; τ_2 is the formation

time for the trapped exciton, essentially the cooling rate in the trapped state well; the ratio C_1/C_2 represents the relative absorption cross sections of the free to trapped excitons at a given wavelength. The long tens of nanoseconds decay of the second species in Eq. (1) is the relaxation time of the trapped exciton back to the ground state.

1. Tunneling—transient absorption of the free exciton

The 8.36 eV free exciton, once created, can be further excited to the Xe conduction band by absorption of a visible photon. If the ionization energy for liquid Xe lies between the measured values of 10.7 eV for a 20 atom cluster[29] and 9.3 eV for the solid,[30] then the free exciton should absorb photons of $\geqslant 1.0$ eV energy. As mentioned above, the oscillator strength is usually greatest near threshold in bound to free ionization transitions; thus, the free exciton transient absorption above ~ 1.0 eV should be greatest at longer wavelengths, and decrease steadily to shorter wavelengths. The steady decrease in the C_1/C_2 ratio with decreasing wavelength shows that indeed, the free exciton absorbance is greater than the trapped exciton absorbance in the red, but smaller in the blue. The absolute absorption intensity of the initial rise at all the wavelengths also appears to increase to the red, further supporting the assignment of the initial absorbing species as the free exciton.

The observed disappearance time of the free exciton τ_1 is the tunneling time for the free exciton to cross the lattice deformation barrier into the trapped exciton well. As expected for the disordered liquid, the observed decay times are very fast, corresponding to tunneling rates on the order of $\sim 5\times 10^{11}$ s^{-1}. The tunneling times also show a slight wavelength dependence, becoming faster to the blue (Table I), indicating a small red shift of the free exciton transient absorption during the tunneling process. This red shift is most likely not a cooling phenomenon; the usual signature of such relaxation is a blue shift of the electronic absorption spectrum, as will be described in further detail below. The 8.4 eV of excitation energy is only 40 meV above the bottom of the free exciton well. Since kT at the temperature of these experiments (280 or 294 K) is ~ 25 meV, significant cooling in the free exciton well should not occur. Furthermore, changing the excitation wavelength to 292 nm, providing 86 meV of additional energy, did not change the observed decay times. If τ_1 corresponded to cooling of the free exciton, increasing the energy of the exciton in the free well should have caused the cooling time to increase. Thus, the red shift associated with the τ_1 process is not the result of cooling and must therefore be an aspect of the tunneling process.

The wavelength dependence of τ_1 must then correspond to tunneling of the free excitons through the barrier at several different points. Tunneling rates depend strongly on the thickness of the barrier at a given well position. If free exciton population is spread throughout the well, then there will be a distribution of tunneling rates. If the fraction of the population in the well at the thinner parts of the barrier absorbs in a different spectral region than those at well locations near thicker parts of the barrier, then the absorption of the free exciton will shift with time. The

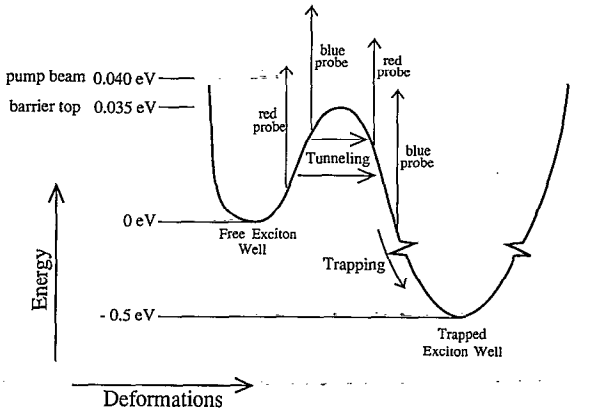

FIG. 6. Energy level schematic showing relative energetics of the free and trapped excitons. After initial excitation into the free well, tunneling to the trapped well can take place through a lattice deformation barrier. Population in the free well near the thinner part of the barrier absorbs to the blue and tunnels faster than population near the thicker part of the barrier, leading to a red shift of the decaying free exciton transient absorption with time. Once tunneling to the trapped well is complete, cooling on a surface similar to that of the xenon excimer (Fig. 5) takes place, leading to a blue shift of the growing trapped exciton absorption spectrum with time.

experimentally measured tunneling rates range from 2.4×10^{11} s^{-1} at 900 nm to 1.1×10^{12} s^{-1} at 500 nm. This observed spectral red shift indicates that the fast tunneling population absorbs to the blue of the slower tunneling population, as depicted schematically in Fig. 6.

2. Trapping—formation and cooling of the trapped exciton

Once tunneling through the lattice deformation barrier is completed, the exciton becomes localized over just a few atomic sites. During this localization, the trapped exciton gives up its excess vibrational energy to the surrounding xenon solvent. The parameter τ_2 in Eq. (1) represents the appearance time for the trapped exciton population after tunneling from the free state well and the subsequent increase in the absorption as the population relaxes down the trapped state well. By noting that the trapped exciton emission spectra was very similar to that of the gas phase excimer, Jortner *et al.* posited that the trapped exciton is localized as a solvated Xe_2^* molecule.[7] Thus, the cooling and associated spectral changes of the trapped exciton should occur in the same fashion as expected for the cooling of a Xe_2^* molecule in liquid xenon. The energetics of the Xe–Xe pair interaction[15] leading to excimer formation in the excited state are shown in Fig. 5.

The vibrational relaxation of a diatomic molecule in a condensed rare gas has been well studied for the case of vibrationally excited I_2 in liquid Xe.[31] In these studies, vibrationally hot I_2 was found to absorb well to the red of the vibrationally cool species; thus vibrational relaxation is characterized by a blue shift of the diatomic transient absorption spectrum. Since the Xe_2^* and I_2 have similar masses and vibrational frequencies (I and Xe are adjacent on the periodic table), it is not surprising that the two species should show similar spectral trends upon cooling in

liquid Xe. The cause of this blue shift for xenon excimers can be seen pictorially in Fig. 5. The vertical transition energy to the first optically accessible electronic excited state ($^3\Pi_g$) for the vibrationally hot ground state ($0_u, 1_u$) excimer species is much smaller than for the vibrationally cool excimers at the bottom of the excimer well. Thus, the absorption spectrum of the Xe_2^* molecules shifts to the blue with time as the population reaches the bottom of the excimer well; that is, the transient absorption spectrum grows in more quickly in the red than in the blue.

This blue shift of the trapped exciton absorption spectrum with time is exactly what is observed in Fig. 2 and summarized in Table I. The clear increase in τ_2 with decreasing wavelength shows that vibrationally hot trapped excitons are appearing more quickly [900 nm, Fig. 2 (i)] than vibrationally equilibrated trapped excitons [500 nm, Fig. 2(a)]. As described above, the trapped exciton is produced by tunneling from different points in the free exciton well. Tunneling through the thinnest part of the barrier produces trapped excitons with more excess vibrational energy than trapped excitons produced from free excitons which tunneled from points lower in the free exciton well (Fig. 6). Thus, the decay of the free exciton species at the thinnest place in the barrier (probed at shorter wavelengths) should correspond to the rise of the vibrationally hottest species in the trapped exciton well (probed at longer wavelengths). This explains why the measured tunneling times are longer than the measured cooling times at the reddest probe wavelengths, and provides a general picture which is consistent with the observed data.

The assignment of τ_1 to the free exciton tunneling decay and τ_2 to the growth and cooling of the trapped exciton is further supported by the existence of the isosbestic point at 810 nm [Fig. 2 (g)]. At this wavelength, the absorption cross sections of the trapped exciton and the free exciton are equal ($C_1/C_2=1$). The tunneling rate for the free species and the cooling rate for the trapped species that absorb this wavelength are also nearly equal (a quick glance at the trends of τ_1 and τ_2 in Table I indicate that $\tau_1 \approx \tau_2$ near 810 nm). Because of these nearly identical rates and cross sections, the resulting absorption at 810 nm is constant with time, as seen from Eq. (1) and Fig. 2(g). The presence of such an isosbestic point is a signature that only two coupled species are involved in the observed absorption kinetics.[32] The isosbestic 810 nm scan indicates that no important intermediates are involved in the dynamics of xenon excitons; thus, only the free and trapped excitonic species are needed to explain all the observed spectral dynamics.

The cooling dynamics of the trapped exciton, however, do not completely follow those expected for a diatomic solvated in liquid Xe. Unlike I_2, which takes several ns to undergo vibrational relaxation in liquid Xe,[31] the trapped xenon exciton is completely cooled within 10 ps. This can be explained by the presence of an additional cooling mechanism which is available to xenon excimers but not to diatomic species like molecular iodine. Since Xe atoms are indistinguishable, it is possible for the electronic excitation to hop from a xenon atom in the excimer to a neighboring xenon atom in the bulk. Martin has constructed a model for trapped exciton cooling in condensed xenon based on resonantly enhanced energy transfer between adjacent xenon atoms.[14] When a bulk Xe atom collides with one of the two excited atoms in the trapped exciton, the excitation will hop from this excited exciton atom to the bulk atom. The exciton now consists of one of its original atoms and the former bulk atom; the other original exciton atom is released into the surrounding medium. This process is illustrated schematically in Fig. 7. For each electronic excitation transfer, a significant fraction of the total excess energy is repartitioned into kinetic energy of the newly created bulk atom; over 0.5 eV of excess energy can be lost in just a few collisions. With this model, Martin predicts trapped exciton cooling times of a few ps,[14] in excellent agreement with the observed results. The density dependence of the cooling rate (Figs. 3 and 4, Tables II and III) is also consistent with Martin's resonant hopping model, as will be discussed in the next section.

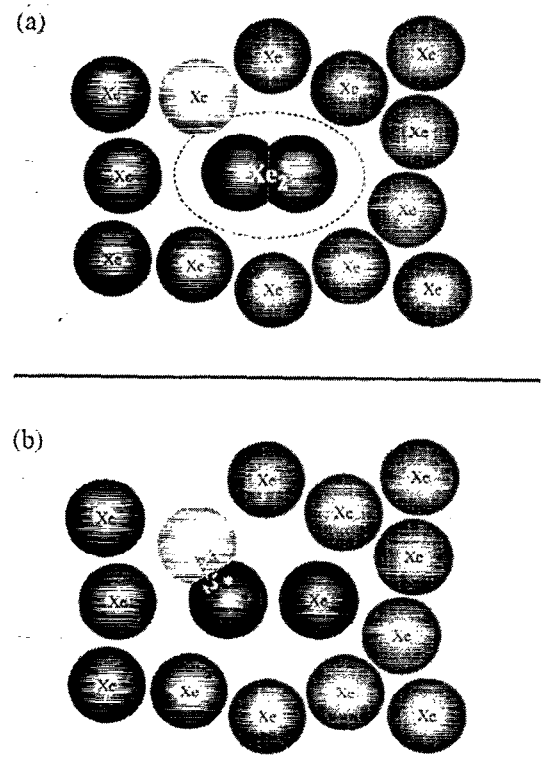

FIG. 7. Schematic illustration of cooling by resonantly enhanced energy transfer between indistinguishable Xe atoms proposed by Martin (Ref. 14). In (a), a Xe atom (light colored) crosses a critical radius for collision (dashed line) with a vibrationally hot Xe excimer (dark atoms). After the new (light) atom crosses this radius, the excitation can hop from the excimer to the new atom, creating a new (mixed color) excimer and releasing one of the atoms formerly in the old (all dark) excimer, as shown in (b). The resonant electronic transfer releases kinetic energy which is taken up by the dark Xe atom in (b), leaving the ("mixed") excimer in (b) vibrationally cooler than the original (all dark) excimer in (a).

C. Density dependence of exciton formation and cooling

Studies of the density dependence of excitonic behavior provide information about the evolution of delocalized ex-

citonic states in the condensed phase from the corresponding isolated atomic states in the gas phase. As described in the Introduction, there exists a critical density at which the average size of clusters in the fluctuating fluid becomes the same as the radius of the delocalized exciton.[10,11,19] For fluid xenon, this critical density for the $\Gamma(3/2)$ $n=1$ exciton occurs at 100 amagats; below this critical density, the $\Gamma(3/2)$ $n=1$ exciton cannot exist.[10] Direct two-photon excitation of fluid xenon below this critical density produces isolated Xe excimers.[27] The vertical two-photon transition produces vibrationally hot excimers at the ground state interatomic separation, as depicted in Fig. 5. The gas phase Xe excimer has an absorption spectrum which spans the visible and near IR.[33] Thus, the transient absorptions presented in this paper should show the behavior of excitons above this critical density and the characteristically different behavior of excited Xe dimers below this critical threshold.

The data of Fig. 3 show that indeed, a marked change in the transient absorption dynamics at 900 nm occurs at densities below 100 amagats. The observed transients at these lower densities can be fit by Eq. (2), a function which characterizes the appearance and decay of a single absorbing species. This is consistent with a picture based on Xe excimer formation. The rapid absorption growth indicates the formation of vibrationally excited Xe_2^* molecules produced directly by two-photon excitation. As these vibrationally hot excimers collide with other Xe atoms and undergo relaxation, their absorption spectrum blue shifts resulting in an absorption decrease at 900 nm. The cooling times for these excimers, given by the τ_4 parameter in Eq. (2) and presented in Table II, are an order of magnitude longer than the cooling times associated with the trapped exciton. Thus, the relaxation mechanism for the cooling of Xe excimers is different from the resonantly enhanced hopping mechanism which describes the cooling of the trapped exciton.

The cooling times of the Xe_2^* molecules scale with density, as would be expected from a relaxation process where single collisions with ground state atoms dominate the relaxation of the excimer. As the density increases, the number of Xe_2^*–Xe encounters per unit time which cool the excimer also increases, leading to a decrease in the relaxation time. As seen in Table II, doubling the xenon density roughly halves the excimer cooling time, in accordance with a picture of isolated single collisions. This type of isolated binary collision cooling mechanism has also been seen for the cooling of molecular iodine[31] as well as for more complex molecules[34] in condensed rare gas solvents. The observed decay rates at the four low densities are more than an order of magnitude slower than the rate at high density, suggesting that below the critical density threshold for exciton formation Martin's cooling mechanism is inefficient.

Unlike the cooling of gas phase excimers, the relaxation rate of trapped excitons does not show any significant dependence on density. Figure 4 (Table III) shows 500 nm transient absorption data taken virtually at the critical density for exciton formation (0.55 g/ml=93 amagats) and at a density three times as great (1.8 g/ml). The fits to these two scans are identical within the noise, showing that density does not significantly alter the tunneling or cooling dynamics of Xe excitons. This is in accord with the resonantly enhanced hopping model of Martin.[14] Martin's calculations show little change in the relaxation rate of the trapped exciton for temperatures ranging from 20 to 150 K; this is due to the fact that the energy loss per resonant energy transfer collision does not depend strongly on density or temperature. Thus, once the critical density for exciton formation is reached, cooling of the trapped exciton proceeds by this mechanism at a rate nearly independent of density. This large change in cooling behavior above and below the critical density for formation of the $\Gamma(3/2)$ $n=1$ exciton further supports the assignment of the observed transients to excitons above the critical threshold and excimers at the lower densities.

V. CONCLUSIONS

We have used picosecond transient absorption spectroscopic techniques to make the first direct measurements of exciton tunneling and trapping in condensed xenon near room temperature. Above the critical density for exciton formation, excitation produces a free $\Gamma(3/2)$ $n=1$ exciton, characterized by a transient absorption which increases continuously to the red. This free exciton decays via tunneling to a trapped state in 1–4 ps. The absorption spectrum of the free exciton shows a slight red shift with time, indicating a distribution of populations with slightly different tunneling rates. Once through the lattice deformation barrier separating the free and trapped exciton wells, cooling of the trapped exciton takes place in roughly 5 ps. This relaxation of the trapped exciton is characterized by a blue shift in its transient absorption spectrum and behaves in a nearly density independent fashion above the critical density for exciton formation. The $\sim$5 ps time scale and the density independence of the trapped exciton cooling rate agree well with a resonantly enhanced excitation hopping model proposed by Martin. Below the critical density threshold for exciton formation, picosecond excitation of compressed xenon creates xenon excimers. These Xe_2^* molecules undergo vibrational relaxation which scales with density in a manner consistent with simple gas phase isolated binary collision models. This work demonstrates the utility of picosecond spectroscopic techniques for study of electronic excitations in condensed rare gases near room temperature where relaxation processes are extremely rapid.

ACKNOWLEDGMENTS

We would like to acknowledge the U.S. Dept. of Energy, Office of Basic Energy Sciences, Chemical Sciences Division under Contract No. DE-AC03-76SF00098 for some specialized equipment used in these experiments. B.J.S. also wishes to acknowledge the National Science Foundation and the W. R. Grace and Company Foundation for their generous support with graduate fellowships.

[1] J. Frenkel, Phys. Rev. **37**, 1276 (1931).
[2] G. H. Wannier, Phys. Rev. **52**, 191 (1937).
[3] R. S. Knox, *Theory of Excitons* (Academic, New York, 1980).
[4] See, e.g., I. Y. Fugol, Adv. Phys. **27**, 1 (1978); R. S. Knox, J. Phys. Chem. Solids **9**, 265 (1959); J. Hermanson, Phys. Rev. **150**, 660 (1966); J. Hermanson and J. C. Phillips, *ibid.* **150**, 652 (1966); D. L. Dexter, *ibid.* **101**, 48 (1956).
[5] J. C. Phillips, Phys. Rev. A **136**, 1714 (1964).
[6] S. A. Rice and J. Jortner, J. Chem. Phys. **44**, 4470 (1966).
[7] J. Jortner, L. Meyer, S. A. Rice, and E. G. Wilson, J. Chem. Phys. **42**, 4250 (1965).
[8] G. Baldini, Phys. Rev. **128**, 1562 (1962); O. Schnepp and K. Dressler, J. Chem. Phys. **33**, 49 (1960).
[9] D. Beaglehole, Phys. Rev. Lett. **15**, 551 (1965); I. T. Steinberger, C. Atluri, and O. Schnepp, J. Chem. Phys. **52**, 2723 (1970); U. Asaf and I. T. Steinberger, Phys. Lett. A **34**, 207 (1971).
[10] P. Laporte and I. T. Steinberger, Phys. Rev. A **15**, 2538 (1977).
[11] P. Laporte, J. L. Subtil, U. Asaf, I. T. Steinberger, and S. Wind, Phys. Rev. Lett. **45**, 2138 (1980).
[12] K. Monahan, V. Rehn, E. Matthias, and E. Poliakoff, J. Chem. Phys. **67**, 1784 (1977); S. Kubota, M. Hishida, and J. Raun, J. Phys. C **11**, 2645 (1978); J. W. Keto, R. E. Gleason, and F. K. Soley, J. Chem. Phys. **71**, 2676 (1979).
[13] R. Kink, A. Lôhmus, and M. Selg, J. Mol. Struct. **61**, 309 (1980); G. Zimmerer, J. Lumin. **18/19**, 875 (1978).
[14] M. Martin, J. Chem. Phys. **54**, 3289 (1970).
[15] T. Suemoto, Y. Kondo, and H. Kanzaki, Solid State Commun. **25**, 669 (1978); T. Suemoto and H. Kanzaki, J. Phys. Soc. Jpn. **46**, 1554 (1979); O. Dössel, H. Nahme, R. Haensel, and N. Schwenter, J. Chem. Phys. **79**, 665 (1983).
[16] R. Kink, A. Lôhmus, and M. Selg, Phys. Status Solidi B **107**, 479 (1981).
[17] B. Raz and J. Jortner, Proc. R. Soc. London Ser. A **317**, 113 (1970); Chem. Phys. Lett. **4**, 511 (1970); A. Gedanken, Z. Karsch, B. Raz, and J. Jortner, Chem. Phys. Lett. **20**, 163 (1973); I. Messing, B. Raz, and J. Jortner, Chem. Phys. **23**, 23 (1977).
[18] H. J. Kmiecik, M. Schreiber, T. Kloiber, M. Kruse, and G. Zimmerer, J. Lumin. **38**, 93 (1987); T. Kloiber, H. J. Kmiecik, M. Kruse, M. Schreiber, and G. Zimmerer, *ibid.* **40&41**, 593 (1988).
[19] J. Wörmer and T. Möller, Z. Phys. D **20**, 39 (1991); T. Möller, *ibid.* **20**, 1 (1991).
[20] H. J. Kmiecik and M. Schreiber, J. Lumin. **37**, 191 (1987).
[21] A more complete discussion of this work can be found in E. S. Peterson, Ph.D. Dissertation, University of California, Berkeley, 1992.
[22] A. L. Harris, M. Berg, and C. B. Harris, J. Chem. Phys. **84**, 788 (1986); M. Berg, A. L. Harris, J. K. Brown, and C. B. Harris, Opt. Lett. **9**, 50 (1984).
[23] W. B. Streett, L. S. Sagan, and L. A. K. Staveley, J. Chem. Thermodyn. **5**, 633 (1973); J. A. Beattie, R. J. Barriault, and J. S. Brierley, J. Chem. Phys. **19**, 1219 (1951).
[24] See, e.g., S. Kubota, M. Hishida, M. Suzuki, and J. Ruan, Phys. Rev. B **20**, 3486 (1979); P. Moutard, P. Laporte, J. L. Subtil, N. Damany, and H. Damany, J. Chem. Phys. **88**, 7485 (1988); N. Böwering, M. R. Bruce, and J. W. Keto, *ibid.* **84**, 709 (1986).
[25] A. W. McCown, M. N. Ediger, and J. G. Eden, Phys. Rev. A **29**, 2611 (1984).
[26] P. Laporte, N. Damany, and J. L. Subtil, in *Photophysics and Photochemistry Above 6 eV*, edited by F. Lahmani (Elsevier, Amsterdam, 1985), p. 289.
[27] W. Gornik, E. Matthias, and D. Schmidt, J. Phys. B **15**, 3413 (1982); D. Haaks, M. Swertz, and J. Schaab, *Photophysics and Photochemistry Above 6 eV*, edited by F. Lahmani (Elsevier, Amsterdam, 1985), p. 413.
[28] *The CRC Handbook of Chemistry and Physics*, 67th ed., edited by R. C. Weist (CRC, Boca Raton, 1986), p. E-77.
[29] L. Cordis, G. Ganteför, J. Hesslich, and A. Ding, Z. Phys. D **3**, 323 (1986).
[30] V. Saile, Appl. Opt. **23**, 4115 (1980).
[31] M. E. Paige and C. B. Harris, Chem. Phys. **149**, 37 (1990); J. Chem. Phys. **93**, 3712 (1990); J. K. Brown, C. B. Harris, and J. C. Tully, *ibid.* **89**, 6687 (1988).
[32] See, e.g., J. E. Huheey, *Inorganic Chemistry*, 3rd ed. (Harper and Row, New York, 1983), p. 303, and references therein.
[33] K. P. Killeen and J. G. Eden, J. Chem. Phys. **84**, 6048 (1986); S. Arai, T. Oka, M. Kogoma, and M. Imamura, *ibid.* **68**, 4595 (1978).
[34] K. E. Schultz, D. J. Russell, and C. B. Harris, J. Chem. Phys. **97**, 5431 (1992).